Journal of Structural Geology 68 (2014) 66–81

Contents lists available at ScienceDirect

Journal of Structural Geology

journal homepage: www.elsevier.com/locate/jsg

Progressive evolution of deformation band populations during Laramide fault-propagation folding: Navajo Sandstone, San Rafael monocline, Utah, U.S.A.

Luisa F. Zuluaga [a, b, *], Haakon Fossen [b, c], Atle Rotevatn [b]

[a] Centre for Integrated Petroleum Research (Uni CIPR), Allégaten 41, 5007 Bergen, Norway
[b] Department of Earth Science, University of Bergen, Allégaten 41, 5007 Bergen, Norway
[c] University Museum of Bergen, The Natural History Collections, University of Bergen, Post Box 7800, N-5020 Bergen, Norway

ARTICLE INFO

Article history:
Received 28 March 2014
Received in revised form
29 August 2014
Accepted 8 September 2014
Available online 21 September 2014

Keywords:
Fault propagation folding
Folding strain
Deformation bands
Laramide contraction
San Rafael Swell
Colorado Plateau

ABSTRACT

Monoclinal fault propagation folds are a common type of structure in orogenic foreland settings, particularly on the Colorado Plateau. We have studied a portion of the San Rafael monocline, Utah, assumed to have formed through pure thrust- or reverse-slip (blind) fault movement, and mapped a particular sequence of subseismic cataclastic deformation structures (deformation bands) that can be related in terms of geometry, density and orientation to the dip of the forelimb or fold interlimb angle. In simple terms, deformation bands parallel to bedding are the first structures to form, increasing exponentially in number as the forelimb gets steeper. At about 30° rotation of the forelimb, bands forming ladder structures start to cross-cut bedding, consolidating themselves into a well-defined and regularly spaced network of deformation band zones that rotate with the layering during further deformation. In summary, we demonstrate a close relationship between limb dip and deformation band density that can be used to predict the distribution and orientation of such subseismic structures in subsurface reservoirs of similar type. Furthermore, given the fact that these cataclastic deformation bands compartmentalize fluid flow, this relationship can be used to predict or model fluid flow across and along comparable fault-propagation folds.

1. Introduction

Porous sandstones tend to develop strain localization features called deformation bands at relatively low strains (Aydin, 1978; Antonellini et al., 1994; Aydin et al., 2006; Fossen et al., 2007). These tabular strain localization structures form by rotation, sliding and crushing of grains, featuring individual thicknesses of less than 1–2 mm, which coalesce into thicker clusters. Individual deformation bands accommodate millimeter-scale offsets that can reach decimeter-scale cumulative offsets in clustered systems. Due to the high porosity required for deformation bands to form (≥15%), they are often associated with (but not restricted to) continental sandstones and burial depths of less than 4 km (Cashman and Cashman, 2000; Shipton et al., 2002; Aydin and Ahmadov, 2009; Brandenburg et al., 2009; Soliva et al., 2013). Deformation bands are interesting for a number of reasons: soon after formation, they "lock-up" and multiply due to strain hardening, recording successive stages of deformation (Davis, 1999b). The strain is usually variably distributed within a deformed volume of porous sandstone (Jamison, 1989) and as they tend to be porosity- and permeability-reducing structures in high quality reservoirs (at micro and meso-scale), they have the potential to either baffle or redirect fluid flow (Antonellini and Aydin, 1994; Fossen and Bale, 2007), creating permeability openings/pathways (Tindall and Davis, 2003; Rotevatn et al., 2009). Deformation band characteristics are thus important for the prediction and assessment of sandstone reservoirs in groundwater/hydrocarbon production, as well as CO_2/water injection (e.g., Sternlof et al., 2006; Rotevatn et al., 2013).

Deformation bands have primarily been described from the extensional regime, where they tend to localize around larger normal faults or form clusters that are interpreted as fault precursors (Aydin, 1977; Aydin and Johnson, 1977, 1978; Antonellini et al., 1994; Hesthammer et al., 2000; Ahlgren, 2001; Shipton and

* Corresponding author. Uni CIPR, P.O. Box 7800, N-5020 Bergen, Norway. Tel.: +47 55 58 36 50 (work), +47 98 99 28 87 (mobile).
E-mail addresses: luisa.zuluaga@uni.no (L.F. Zuluaga), haakon.fossen@geo.uib.no (H. Fossen), atle.rotevatn@geo.uib.no (A. Rotevatn).

http://dx.doi.org/10.1016/j.jsg.2014.09.008
0191-8141/

Cowie, 2001; Torabi and Fossen, 2009; Tueckmantel et al., 2010; Schueller et al., 2013). In contrast, studies of deformation bands formed in the contractional regime are less commonly reported in the literature (cf. Davis, 1999b; Cashman and Cashman, 2000; Wibberley et al., 2008). Solum et al. (2010) and Brandenburg et al. (2012), based on observations from the East Kaibab monocline on the Colorado Plateau, suggested that contraction-induced deformation bands may be more broadly distributed away from faults, while the ones formed during extension are more localized (i.e. narrower damage and process zones of main faults), hence affecting fluid flow in a different way. Other studies (Ballas et al., 2012a; Soliva et al., 2013) analyzed deformation bands formed during contraction and extension phases in the South-East Basin in southern France, suggesting that whereas contraction-induced deformation bands are more widely distributed, extension-related deformation bands affected paleofluids to a greater extent. On the contrary, Saillet and Wibberley (2013) found no noticeable relationship between tectonic regime and band permeability for the same region.

These contrasting results indicate that tectonic regime is only one of several factors influencing the role of deformation bands in reservoirs (e.g., Fossen and Rotevatn, 2012); wider spatial distribution of deformation bands throughout contractional structures seems to be a common observation, but more information is needed to explore more closely the role of deformation bands during shortening of porous sandstones, and to characterize and evaluate their effects on fluid flow.

In this study we focus on a particularly well-exposed example of folded porous Navajo Sandstone on the Colorado Plateau, the Laramide San Rafael monocline in southeastern Utah, which is particularly well suited for studies of deformation band formation in a contractional setting. Structural mapping along several parallel canyons that transect the structure allows us to compare differently dipping forelimb sections, and compare the distribution and characteristics of deformation bands with respect to dip or fold tightness. Because deformation band development depends on strain (Bésuelle, 2001), the relationship between strain and deformation band type, organization and distribution can be assessed in this field example. Our observations allow us to propose a sequence of deformation band development through time. The main aim of this study is thus to elucidate how strain, in the form of potentially flow-altering deformation bands, is distributed in contractional folds. This is achieved through the following set of objectives, which are i) to describe and characterize deformation bands formed during contractional folding in terms of geometry, distribution and petrophysical properties, ii) to propose a model for the formation and evolution of deformation bands during such folding, and iii) to establish a relationship between forelimb dip (interlimb angle) and deformation band density, ultimately allowing us to iv) discuss applications with respect to analog reservoir settings.

2. Geologic setting

The study area lies in the Colorado Plateau of the southwestern U.S.A.; a region characterized by relative crustal stability and thick-skinned tectonics, mainly in the form of basement uplifts (Davis, 1999b). The focus of this study, the San Rafael monocline (SRM) is located 25 km west of Green River in Utah, forming the eastern flank and the most steeply dipping layers of the doubly-plunging asymmetric San Rafael Swell (SRS), ~120 km long and 60 km wide (Fig. 1). The SRM exhibits maximum inclinations of ~65°, flattening laterally both to the north and south, where it evolves into gentle homoclines, strikes approximately N20°E in its northern part, and N50°E in its southern part. The structure is interpreted to have formed during the well-documented Late Campanian-Eocene Laramide contractional deformation event, the youngest reverse reactivation of high-angle normal faults in the Precambrian basement (Rigby, 1987; Neuhauser, 1988; Johnson and Johnson, 2000; Bump and Davis, 2003; Fischer and Christensen, 2004; Cross, 2009). The SRM has been interpreted as a forced fold (Stearns

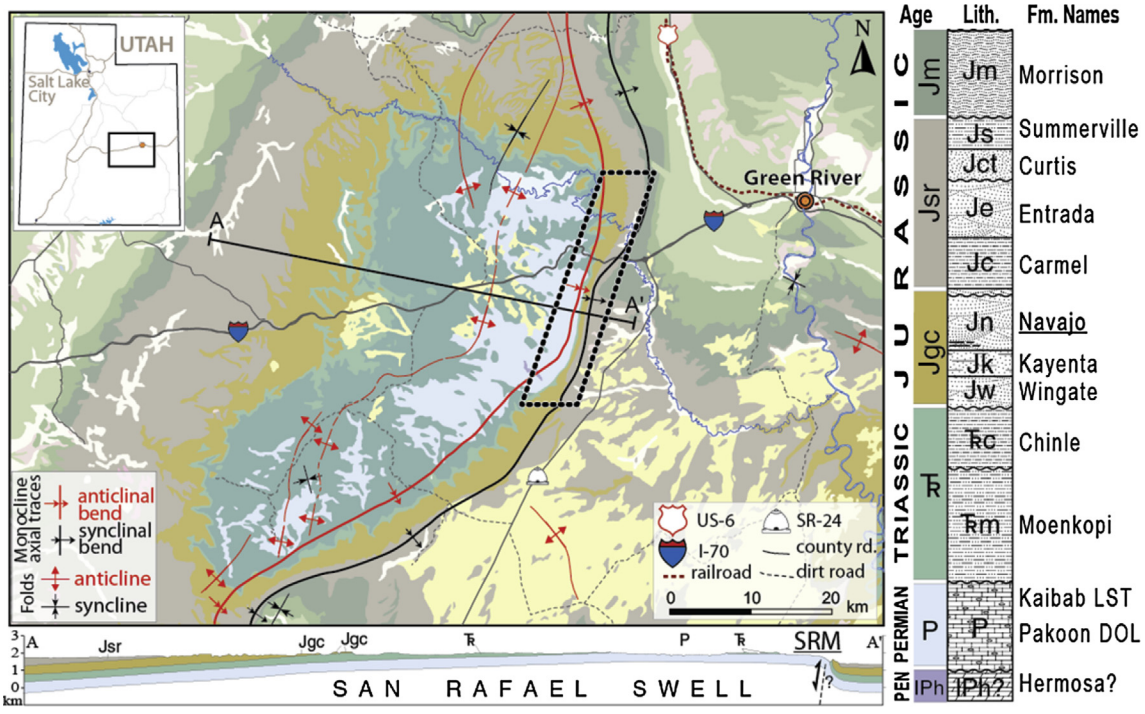

Fig. 1. Stratigraphic column, geologic map and cross section of the San Rafael Swell and San Rafael monocline (SRM). Units as old as Permian outcrop in the fold core (light blue). Sub-region with contraction-deformation band populations is delimited by the dashed polygon along the steepest segment of the monocline. (For interpretation of the references to color in this figure legend, the reader is referred to the web version of this article.)

and Jamison, 1977) or a fault propagation fold (Bump and Davis, 2003; Davis and Bump, 2009) controlled by a blind fault with pure thrust-slip or reverse-slip kinematics. This reactivated fault offsets Precambrian to Paleozoic rocks, folding the overlaying Mesozoic sequence. Although the underlying SRM fault does not crop out, and crossing seismic profiles fail to image it, possibly due to its steep dip (Allmendinger, 1992), more deeply eroded Laramide uplifts on the Colorado Plateau with similar structural character expose fault tips within the Upper Paleozoic sequence (Huntoon, 1993; Tindall, 2000; Karlstrom and Timmons, 2012), and a similar termination is expected for the SRM.

In terms of tectonic and depositional history, the main events leading to the current SRM configuration are described in Fig. 2. For a detailed account of Paleozoic evolution, see Herman and Sharps (1956), Huntoon (1993), Huntoon et al. (1994), Condon and Huffman (1997), Marshak et al. (2003), Miall and Blakey (2008), Blakey and Middleton (2012), and see Dickinson and Snyder (1978), Dumitru et al. (1994), Goldstrand (1994), Bjerrum and Dorsey (1995), Allen et al. (2000), DeCelles and Coogan (2006), Cross (2009), Jones et al. (2011) for the Mesozoic and Cenozoic evolution, including Laramide deformation.

2.1. Navajo Sandstone

The rocks outcropping along the SRM range in age from Permian in the fold core to Upper Cretaceous along the outer limbs (Fig. 1). In the study area, the Jurassic Navajo Sandstone, ~120–200 m thick, is exposed continuously along strike, in cliffs dissected by several slot canyons that cut into the monocline. This unit is composed of cross-bedded, white to tan weathered, well-rounded, well-sorted, and fine-to medium-grained quartz-rich sandstone deposited in eolian settings during the Lower to Middle Jurassic (Fischer and Christensen, 2004). The Navajo Sandstone has undergone burial to around ~2 km for the east Kaibab monocline southwest of the SRM (Fossen et al., 2011) and 2.8 km some 30 km east of the SRM (Davatzes et al., 2003). Exhumation began at around 50–35 Ma (Nuccio and Condon, 2000) from burial depths that are too shallow to promote significant quartz dissolution (Fossen et al., 2011).

Because of its high porosity and good sorting, the Navajo Sandstone is also found to develop deformation bands easily where deformed by folding or faulting (e.g., Antonellini and Aydin, 1994; Shipton and Cowie, 2001; Fossen et al., 2010). At present, porosity is about 20% and permeability reaches 3.5 darcy (this study). Hence, the Navajo Sandstone and its lateral equivalents are widely recognized as reservoirs for both groundwater and oil, for instance in the Covenant oil field on the west side of the SRS (Beitler et al., 2003; Parry et al., 2009). In the study area, paleo-fluid flow can be inferred from the abundant bleaching patches throughout the Navajo Sandstone, in which some spots of iron oxide and carbonate cementation can be identified (Beitler et al., 2005).

3. Methodology

3.1. Data acquisition and analysis

In order to evaluate the characteristics and spatial distribution of deformation bands, field observations relating to geometric and petrophysical properties were made in the Navajo Sandstone along

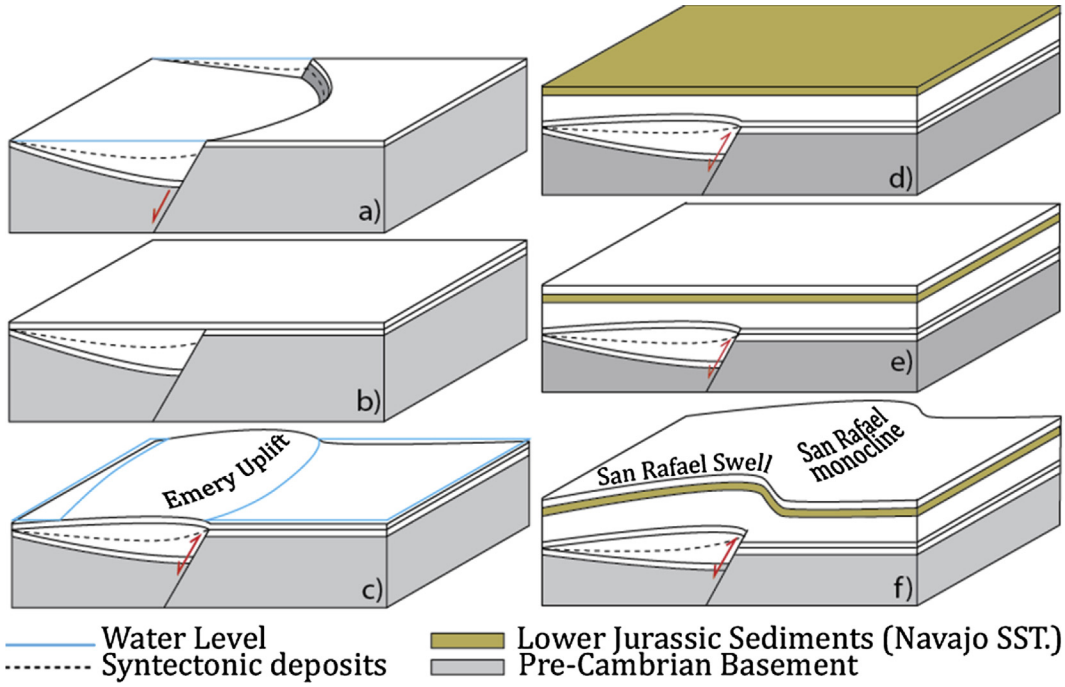

Fig. 2. Block diagram with simplified tectonic evolution, see text for references: a) Precambrian Rifting, the mainly west-dipping extensional basement faults beneath Laramide uplifts originated during Neo-Proterozoic rifting along the western margin of North America NAM (~650 Ma). Subaqueous syn-rift deposition accompanied rifting, b) Lower Paleozoic quiescence, in early Paleozoic times, post-rift sediments started to accumulate on the passive margin. c) Middle Paleozoic inversion: at the end of Paleozoic, mountain ranges of the Ancestral Rocky Mountain orogeny began forming at east (ARM), and a gentle shallow marine uplift developed (the Emery Uplift) to which the San Rafael Swell has been associated. This uplift limited sea water influx at low sea levels, controlling sediment thicknesses at increasing water depths. d) Mesozoic deposits (lower Jurassic highlighted). After the Uncompahgre Highlands of the ARM became fully inactive, they were steadily eroded, providing additional sediment sources that progressively buried the Emery Uplift. e) As the sea receded in the Mesozoic, convergence and subduction at the NAM created the Nevadan Orogenic Belt, forming a foreland basin in the east, in which extreme arid conditions allowed the widespread deposition of eolian units including the Navajo Sandstone in the Lower/middle Jurassic. f) Laramide inversion, formation of San Rafael Swell and its forelimb, the San Rafael monocline. The continuing collision between the NAM and the Paleo-Pacific plate created the arc complex of the Sevier Orogen, followed by the mostly Tertiary (Eocene) Laramide orogeny as a farther-inland contractional reactivation of the initial Precambrian basement faults, during which the San Rafael Swell and other uplifts of the Colorado Plateau formed. Finally, the uplift and erosion of the Colorado Plateau exposed units as old as Permian on the crest of most Laramide uplifts.

the San Rafael monocline in canyons dissecting the fold (Fig. 3). Moving along strike from steeply-to shallowly-dipping sandstone, it was possible to demarcate and map the zone in which deformation bands are present. Deformation band observations were then related to the local dip of bedding: steep (65°–52°), intermediate (51°–32°) and gentle (31°–20°).

Among the localities studied, ten contained significant deformation band populations (Fig. 4). At each locality, deformation band orientations were measured, and bands were further subdivided into categories according to their type, geometry and arrangement of arrays, establishing their relative positions within the sandstone interval and the fold.

To evaluate frequency and spatial distribution of deformation bands in the Navajo Sandstone in the study area, observations and measurements were recorded for single or individual bands and deformation band zones. For single deformation, scan lines were used to assess deformation bands intensity (number of bands per meter) along layer-normal and layer-parallel traverses along the canyon walls. At a somewhat broader scale, deformation band zones, visually identifiable from a wider field of view, were counted as single zones, each consisting of an array of deformation bands. Quantitative spatial data collection from such zones were collected remotely by using triangulations from laser range finder measurements to estimate length and continuity across bedding, thickness of arrays, and angular and spatial relationships of sets of the same type. This allowed us to estimate zone spacing also in otherwise inaccessible canyon walls.

Examination of satellite imagery from Google Earth allowed us to relate detailed field observations to the km-scale size of the monocline. Photographs at different scales of observation were taken and sketched to refine all observations, and to compare different localities. Extraction of elevation profiles from DEM combined with referenced geological maps allowed the construction of cross-sections of the steepest sectors of the forelimb in which deformation bands and spatial distribution of arrays were outlined.

To evaluate petrophysical properties of the deformed as well as the undeformed sandstone, permeability measurements were done in the field using a portable air permeameter (TinyPerm II by NER), the technical details of which are described in Filomena et al. (2014). Measurements were carried out parallel to bedding from

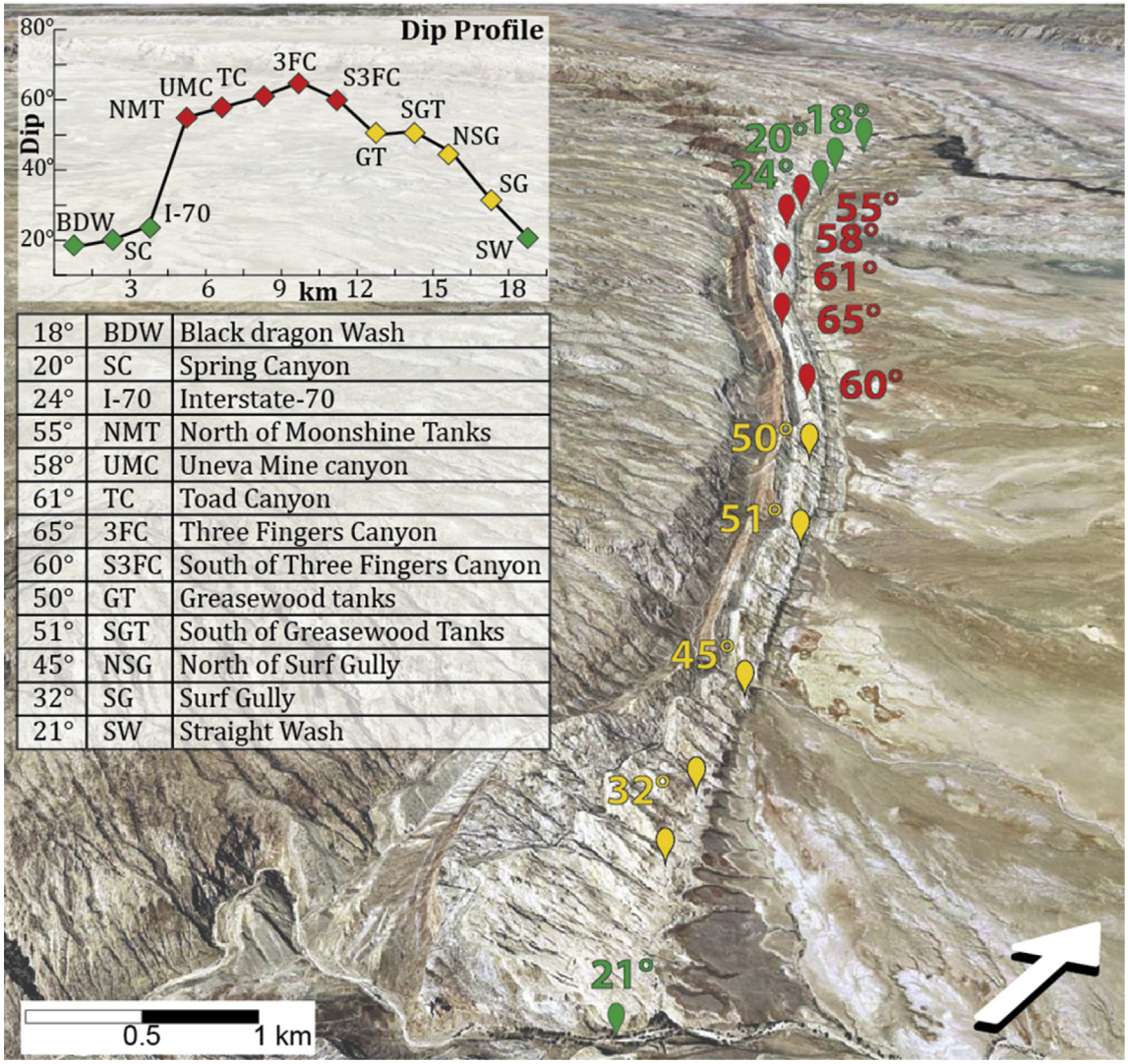

18°	BDW	Black dragon Wash
20°	SC	Spring Canyon
24°	I-70	Interstate-70
55°	NMT	North of Moonshine Tanks
58°	UMC	Uneva Mine canyon
61°	TC	Toad Canyon
65°	3FC	Three Fingers Canyon
60°	S3FC	South of Three Fingers Canyon
50°	GT	Greasewood tanks
51°	SGT	South of Greasewood Tanks
45°	NSG	North of Surf Gully
32°	SG	Surf Gully
21°	SW	Straight Wash

Fig. 3. Google Earth view of the San Rafael monocline SRM, showing field localities and corresponding gentle, intermediate and steep dip domains of the fold (in green, yellow and red respectively). Top left: graph showing the dip variation along strike across canyons; notice the rapid dip increase in distances of less than 3 km along strike. Table with locality names, abbreviations and associated Navajo dips. Cairn Canyon and Iron Wash field localities from Davis (1999b) and Bump and Davis (2003) correspond in this paper to Three Fingers Canyon 3FC and Straight Wash SW, respectively, according to USGS topographic maps for the area (BLM and USGS, 2005). (For interpretation of the references to color in this figure legend, the reader is referred to the web version of this article.)

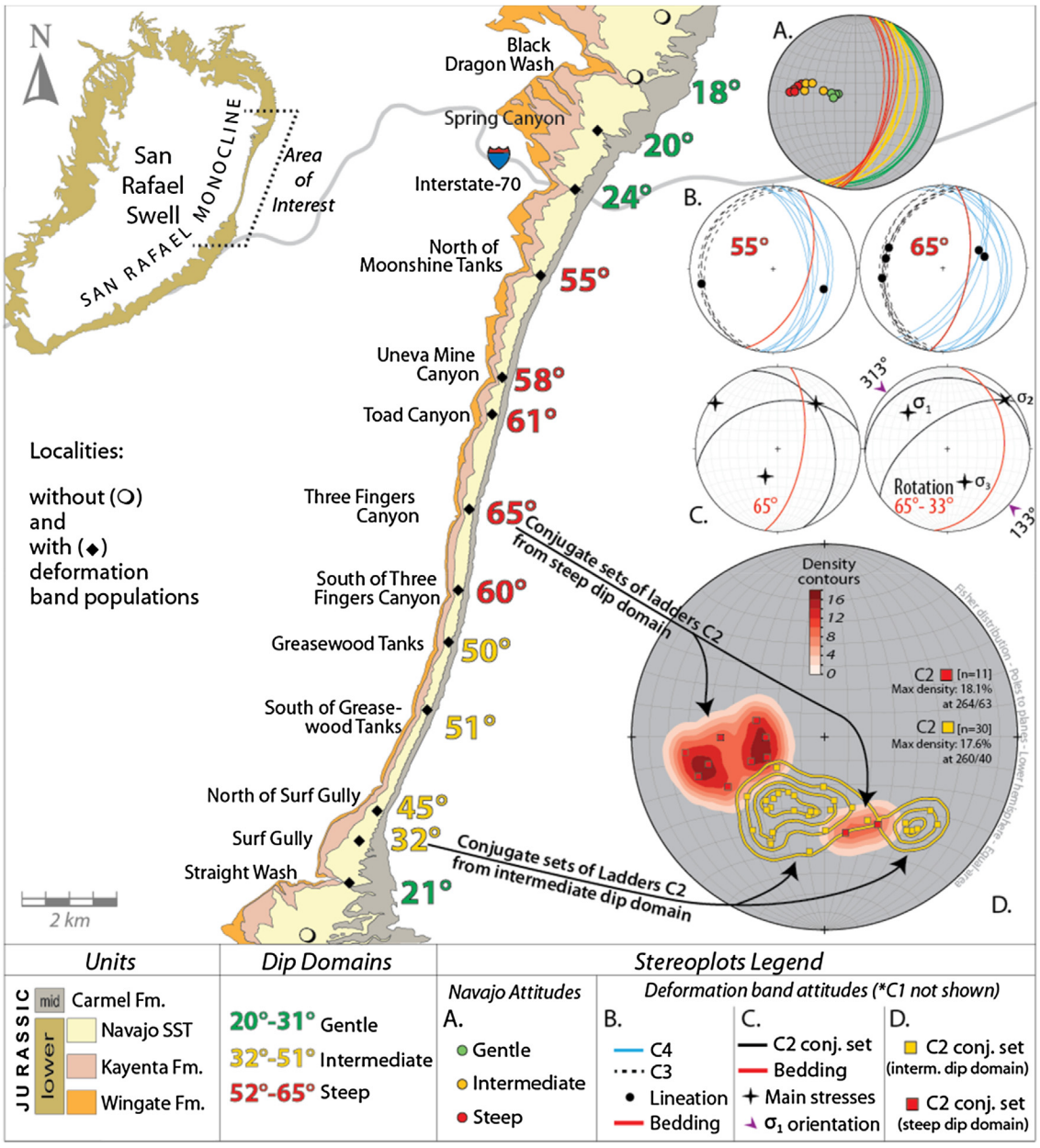

Fig. 4. Detail of localities and orientations for the study area. A. Poles and planes of bedding attitudes for the Navajo SST along SRM localities. B. Selected orientation data and associated lineations of slip surfaces (C3) and tabular clusters (C4), in steep dip domain localities: NMT, 55° (left) and 3FC, 65° (right). For C3, rotation and spread is more evident. C. Selected conjugate set of ladder zones (C2) and poles to plane bisectors (main strain axis) from the steepest dip locality (3FC, 65°); right: rotation from the stereonet at left, to reach an intermediate 32° dip (i.e. dip where C2 ladders start developing) with resulting stress orientations. D. Comparison between poles to planes and contours of conjugate sets of ladder zones in intermediate (yellow) vs. steep (red) dip domains, showing steepening (rotation) of the point clouds. (For interpretation of the references to color in this figure legend, the reader is referred to the web version of this article.)

the base to the top of the Navajo Sandstone at excavated fresh surfaces of rock. Measurements were recorded from intact host rock as well as from deformation bands in order to capture variations and contrasts in permeability. In the steepest segment of the fold, rock samples were collected to study the micro-texture of host rocks and deformation bands using thin sections.

The permeability measurements were separated into three groups: i) intact host rock, in areas devoid of deformation bands ii) host rock contained within networks of deformation bands iii) direct measurements across deformation bands (where measurable surfaces were exposed).

In this paper we use the classification of deformation bands of Fossen et al. (2007), and favor the usage of the descriptive term ladder structures by Schultz and Balasko (2003) although we realize that the geometry of the ladder structures in this area is consistent with a kinematic as Riedel shear zones as used by Davis et al. (2000) and (Ahlgren, 2001).

4. Structural observations

Deformation bands are restricted to a 16 km long zone along the hogbacks south of Interstate I-70 and west of highway SR-24, i.e. the steepest-dipping part of the SRM (Figs. 3 and 4). The steepest dips of the Navajo sandstone (65°) occur around the Three Fingers Canyon locality, decreasing along strike toward north (24° at I-70) and south (21° at Straight Wash locality). For simplicity, the study

area was subdivided into gentle (20°–31°) intermediate (32°–51°) and steep (52°–65°) dip domains (Fig. 4). These ranges are defined according to the occurrence of the different deformation band structures, and discussed in Section 4.2. In terms of interlimb angle, the steep, intermediate and gentle dip domains of the SRM would correspond to interlimb angles of 115°–128°, 129°–148° and 149°–160°, respectively.

Outside the study area, populations of cataclastic deformation bands are mainly associated with normal faults that crosscut and thus postdate the SRM, first described by Aydin and Johnson (1978) in the nearby San Rafael desert, and subsequently in the same area by Fossen and Hesthammer (1997) and Johansen and Fossen (2008). These extensional bands are not found in the study area. There are also soft-sedimentary disaggregation bands in several places in the Navajo Sandstone, easily distinguished from the cataclastic bands related to the SRM folding (see Fossen et al., 2007 for classification), and thus excluded from the descriptions below.

4.1. Deformation bands

Individual deformation bands in the study area are cataclastic, white, and rarely exceed 1 mm in thickness; cumulative thicknesses of deformation band assemblages can reach 1.5 m depending on the type of array they are part of. The bands are barely protruding from the surrounding host rock, contrary to the fault-fin landscapes described elsewhere (Antonellini et al., 1994; Davis, 1998; Saillet and Wibberley, 2010; Fossen et al., 2011). Single deformation bands represent zones of intense cataclasis and local cementation, some being exclusively composed of crushed quartz grains, while others contain additional ferruginous material between the crushed quartz grains (Fig. 5). Fracturing at grain contacts generate grains that are angular as compared to the more rounded grains in the host rock, which are characterized by concave-convex and planar grain boundaries and higher porosities (~20%). Occasionally, rare patches of calcareous and ferruginous cement are observed. Where bedding can be traced, single deformation band offsets are in the range of 0.5–3 mm, while band arrays may offset bedding by as much as 0.5 m.

4.2. Deformation band arrays

Cataclastic deformation band arrays in the SRM along the Navajo sandstone can be grouped into four categories based on their geometry and occurrence in the field: **C1**, bedding-parallel deformation bands; **C2**, oppositely-dipping conjugate sets of deformation bands arranged in ladder structures; **C3**, deformation band zones bounded by slip surfaces, and **C4** densely packed deformation band strands in tabular clusters.

C1: Bedding-parallel deformation bands follow depositional boundaries, crossbeds and bounding surfaces (Fig. 6A). Crossbed-parallel band thickness ranges from 1 mm (single) to 1 cm (clustered), while bands along bounding surfaces are up to 10 cm thick. There is not a uniform spacing between bands in this category inside of each duneset, however they are more common near the top of the dunesets; **C2: Oppositely-dipping conjugate sets of deformation band zones**, arranged in ladder structures, hereafter called **ladder zones** for simplicity, which occur across bedding throughout the entire Navajo interval. Similarly-oriented sets of ladder zones are 3–5 m apart, but vary in thickness from less than 10 cm to 1 m. These arrays define semi-brittle shear zones with step-over geometries, with long and planar bounding bands (flanks) connected via short linking bands (rungs), as described by Okubo et al. (2006). Oppositely dipping sets of ladder zones have acute angles of up to 45° with sub-horizontal bisectors between them, whereas within each set, angles between bounding bands and linking bands vary from acute to perpendicular (Fig. 6B, C); the acute bisector angles for ladder zones are smaller than the 60° typically quoted for conjugate sets, but still define the horizontal principal stresses, and are in accordance with conjugate deformation band sets reported elsewhere (Aydin and Reches, 1982; Zhao and Johnson, 1992; Du Bernard et al., 2002); **C3: Deformation band zones bounded by slip surfaces**, spaced 1.5–3 m apart (Fig. 6D), equivalent to the thrust-slip deformation band shear zones of Davis (1999a), always at the base of the Navajo; and finally **C4: Densely packed tabular clusters of deformation band strands**, in which all individual deformation bands are parallel to each other and coalesce into a thick inosculating zone of deformation bands that occur sub-parallel to and nearly at the top of the Navajo Sandstone only, independent of sedimentary structures, with total thicknesses of up to 0.2 m (Fig. 6E).

In terms of kinematics, sense of shear is mainly observable for categories 2 and 3 with bedding offsets of as much as 0.5 m, mainly reverse-sensed, although normal displacement ladder zones do occur, especially near the top of the formation. Band Category 1 and 4 are (sub-)parallel to bedding, thus offset and sense of shear are difficult to estimate. Table 1 shows a summary of deformation bands characteristics with respect to band category. Categories 1 to 4 are all present in the steepest section of the monocline, reducing in thickness and intensity into the intermediate and gentle dip domains, where only Category 1 is present, until ultimately, no contraction-related cataclastic deformation bands occur.

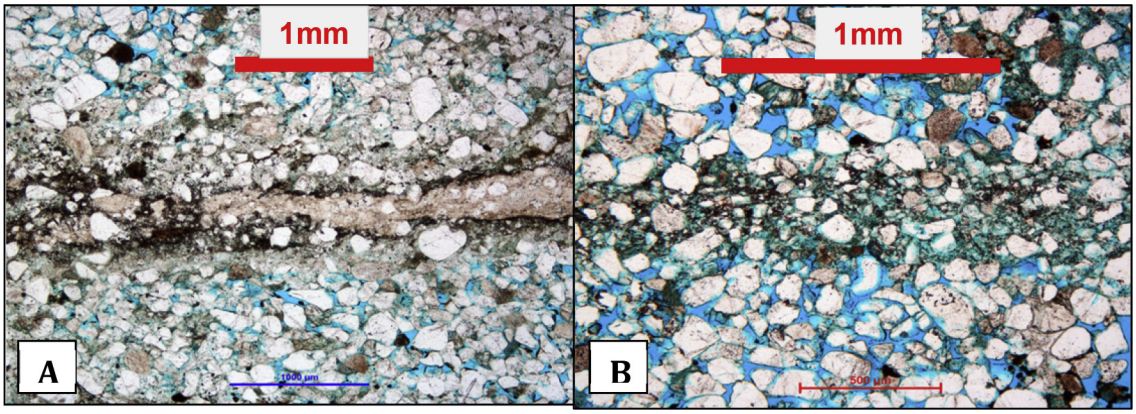

Fig. 5. Microscope images of single deformation bands. Notice grain size reduction due to crushing (Cataclasis). Little or no porosity remains from cataclasis and introduction of ferruginous material in the deformation band at left (A), while some porosity is preserved in the deformation band at right (B).

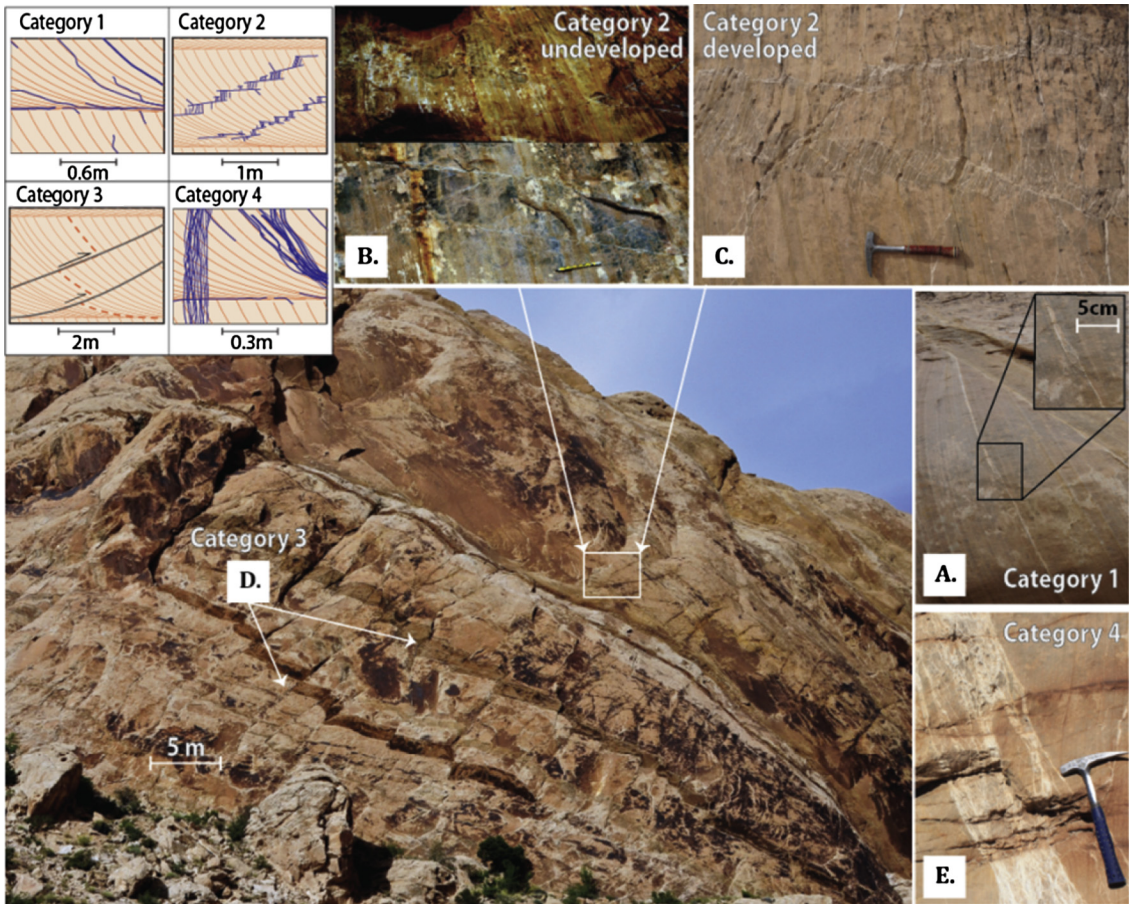

Fig. 6. Deformation band arrays in the SR monocline. A. Category 1, bedding-parallel/sub-parallel cataclastic bands (notice jump across crossbeds with hook shaped tips); B and C. Category 2 (ladder zones) incipient (B, pen for scale) and developed conjugate set (C); D. Category 3 (slip surfaces) and E: Category 4 (tabular cluster). Top left: drawing showing simplified sketches of deformation band types: Category 1, bedding-parallel/sub-parallel. Category 2, ladder zones (only one set shown). Category 3, slip surfaces (due to the scale of observation) the surrounding deformation bands are not drawn. Category 4 clusters of deformation bands. (Top of Navajo at right border of the rectangles.)

Slip surfaces (Category 3) and tabular clusters (Category 4) were found only in the steepest dip domains of the fold (52°–65°). Additionally, Category 3 was only found in the stratigraphically lowermost part of the Navajo Sandstone, whereas Category 4 is restricted to the uppermost part. In terms of orientation, slip surfaces (C3) strike N–S and dip ~30° to the west, while tabular clusters (C4) are sub-parallel to the top of the Navajo Sandstone.

Bedding-parallel deformation bands (Category 1) and conjugate sets of ladder zones (Category 2) on the other hand, cover almost the entire sandstone interval along strike and across sub-layers in the Navajo Sandstone. Since band orientations of Category 1 structures are controlled by sedimentary structures (dunesets, laminae and individual crossbeds), they vary greatly in orientation. In contrast, orientations of conjugate sets of ladder zones of Category 2 strike mainly NNE and SSW, with respectively W and E dip directions, and acute bisector angles of 35°–45° (Fig. 4C, D). There is some variation, however, with respect to stratigraphic position: west-dipping ladder zones dominate toward the base of the formation, while east-dipping ladders become more prominent toward the top, where some of them exhibit normal offset.

4.2.1. *Gentle dip domains (20°–31°)*

Spring Canyon, I-70, and Straight Wash localities (Fig. 4): These dip domains have very rare bedding-parallel cataclastic deformation bands (Category 1), usually in the form of single bands or a few tightly clustered bands (Fig. 6A). Individual deformation bands in this domain never surpass a few millimeters of thickness and cm-scale offsets. The bands can reach several meters in length as

Table 1
Spatial characteristics of deformation band arrays in the San Rafael monocline.

Category	Thickness	Spacing (m)	Length		Continuity		Connectivity	DIP domain		
			Along strike (m)	Across layering (m)	Along strike	Across layering		Gentle	Intermediate	Steep
C1	1 mm –10 cm	Not uniform	≤10	[a]	Good	Poor	Good	☑	☑	☑
C2	10 cm–1.5 m	3–5	5–10	10–50	Moderate	Good	Moderate		☑	☑
C3	1–5 cm	1.5–2.5	[a]	15–20	[a]	Poor	None			☑
C4	1 mm–50 cm	Not uniform	≤20	[a]	Moderate	Poor	Moderate			☑

[a] Uncertain.

they follow duneset boundaries or crossbeds. Their height is limited by the fact that they are locally arrested or bifurcate at stratigraphic boundaries.

4.2.2. Intermediate dip domains (32°–51°)

Localities belonging to the intermediate dip domains are Surf Gully, North Surf Gully, South Greasewood Tanks, and Greasewood Tanks (Fig. 4). At these localities, bedding-parallel deformation bands (Category 1) are more frequent than in the gentle dip domain, reaching up to 1 cm in thickness and several meters in length. These bands connect with hook-shaped tips (Fig. 6A), showing that they formed at individual locations and interacted as they propagated. They consistently follow crossbeds but can locally jump across bedding to adjacent laminae within the same duneset. Usually these deformation bands terminate at duneset boundaries. In addition, millimeter-thick and decimeter-long sets of deformation bands of Category 2 (ladder zones) occur at high angles to bedding. These single bands are discontinuous, but locally portray overlap zones or step-overs that may represent incipient ladder structures (Category 2 Fig. 6B). In general, it is possible to identify two conjugate sets of ladder zones bisected by acute angles (35°–45°) throughout this dip domain, one set dipping west and the other varying between sub-horizontal and gently east-dipping orientations.

Overlapping deformation bands in ladder zones of Category 2 start to develop semi-brittle shear zones in the stepover area, mainly offsetting bedding in a reverse sense, although some ladder zones with normal offsets do occur. These semi-brittle shear zones evolve into complex ladder structures (Fig. 6C), which can offset bedding by as much as 0.5 m, and are more frequent and better developed as the fold steepens (see next domain).

4.2.3. Steep dip domain (52°–65°)

The steepest dipping beds are found in North of Moonshine Tanks, Uneva Mine Canyon, Toad Canyon, Three Fingers Canyon, and South Three Fingers Canyon (Fig. 4). In these localities the full range of deformation band categories is observed. Categories 3 and 4 are in these localities restricted to the base and top of the Navajo Sandstone, respectively. The discrete slip surfaces (Category 3) show reverse offsets of up to 0.5 m, dipping up to ~30° toward west (Fig. 6D).

Ladder zones (Category 2) are more numerous, thicker and more complex, aggregating abundant deformation bands in both the overlaps and their surroundings, and showing higher shear offset (Fig. 6C). The conjugate set of ladder zones recognized in the intermediate dip domains is also present here. In the steep dip domain, however, the west-dipping set is dominant toward the base of the Navajo Sandstone, while the east-dipping to sub-horizontal set becomes more noticeable near the top. Ladder zones reach a maximum of 1 m in thickness (i.e. thickness of the zone encompassing all the individual deformation bands), while Category 1 (bedding parallel) structures are not much thicker than in the preceding domains, although they are more common. Clusters of Category 4 deformation bands are sub-parallel to/and appearing at the top of the formation, where they reach up to 0.2 m in thickness (Fig. 6E).

4.3. Spatial distribution of deformation bands in the SRM

4.3.1. Length and spacing

Deformation bands of Category 1 (bedding parallel) are typically arrested at locations of stratigraphic heterogeneity, such as differently oriented crossbeds or dune boundaries. Additionally, they are consistently offset by deformation bands that transect bedding. Ladder zones (Category 2) extend for several tens of meters across bedding, and define sets that are spaced in the range of 3–5 m. Deformation bands of Category 3 and 4 are present only at the base and top of the Navajo Sandstone, respectively. Slip surfaces of Category 3 tend to terminate at the first major bounding surface in the sandstone, but are fairly continuous within the bottom sub-

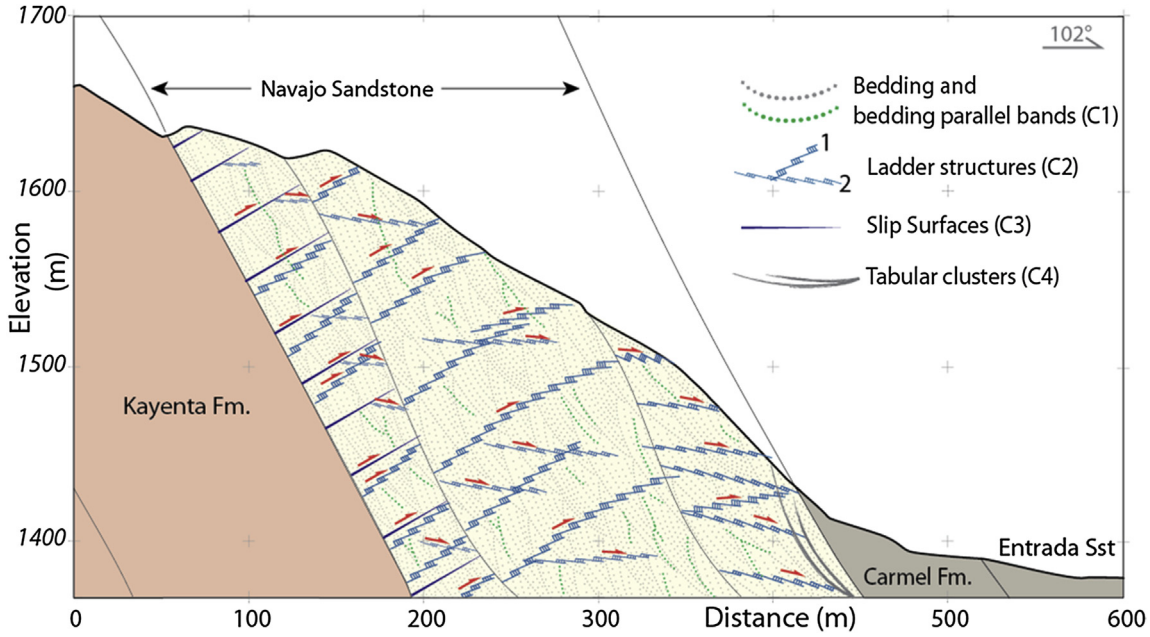

Fig. 7. Cross-section across a steep dip domain in the SRM (~62°), showing types and spatial distribution of deformation band arrays in the Navajo sandstone. Category 1: bedding-parallel deformation bands; Category 2: conjugate sets of ladder structures with mostly reverse sense of shear, west-dipping set dominates towards the base, east-dipping towards the top (both consistently offset C1); Category 3: reverse sensed and top to the east slip surfaces at the base of the Navajo sandstone, restricted to the first bounding surface from base to top. Category 4: sub-parallel deformation band clusters near the top of the formation. Spacing between arrays is exaggerated about ten times compared to the real spacing in the outcrop.

layer where they are spaced on average 1.5–2.5 m apart; tabular clusters of Category 4 are visible only in the first few decimeters from the top of the Navajo Sandstone (Fig. 7). Lateral continuity along strike is difficult to estimate for all categories, but correlations across the slot canyons suggest a minimum length of several tens of meters for both ladder zones of Category 2 and clusters of Category 4.

4.3.2. Deformation band array intensity relative to fold geometry

In order to quantify the relationship between deformation band density and layer orientation (dip of the forelimb of the monocline), scan-line observations across the Navajo Sandstone were plotted from locations shown in Fig. 4. Bedding dip was recorded along with scanline data to understand the relationship between band occurrence and dip. Fig. 8 shows that the number of bedding-parallel deformation bands increases with increasing forelimb dip. The minimum and maximum values of frequency for bedding-parallel deformation bands are 0.1 bands/m (i.e. an average band spacing of 10 m) in gentle domains, and the maximum is 11.7 bands/m (i.e. an average band spacing of ca. 8.5 cm) in the steepest sector of the forelimb. In Fig. 8A, single bands as well as tight clusters of multiple bands (2–5) are counted as single occurrences. Ladder zones show a more linear increase in frequency with increasing limb dip (Fig. 8B), with a first occurrence at ~32° forelimb dip and reaching a maximum of 1 ladder zone per meter at 60°.

5. Permeability and porosity measurements

At each locality, probe permeability measurements were taken along bedding in intact host rock, in host rock in between deformation band arrays and deformation band planes. Measurements were independent from deformation band categories, aiming for an

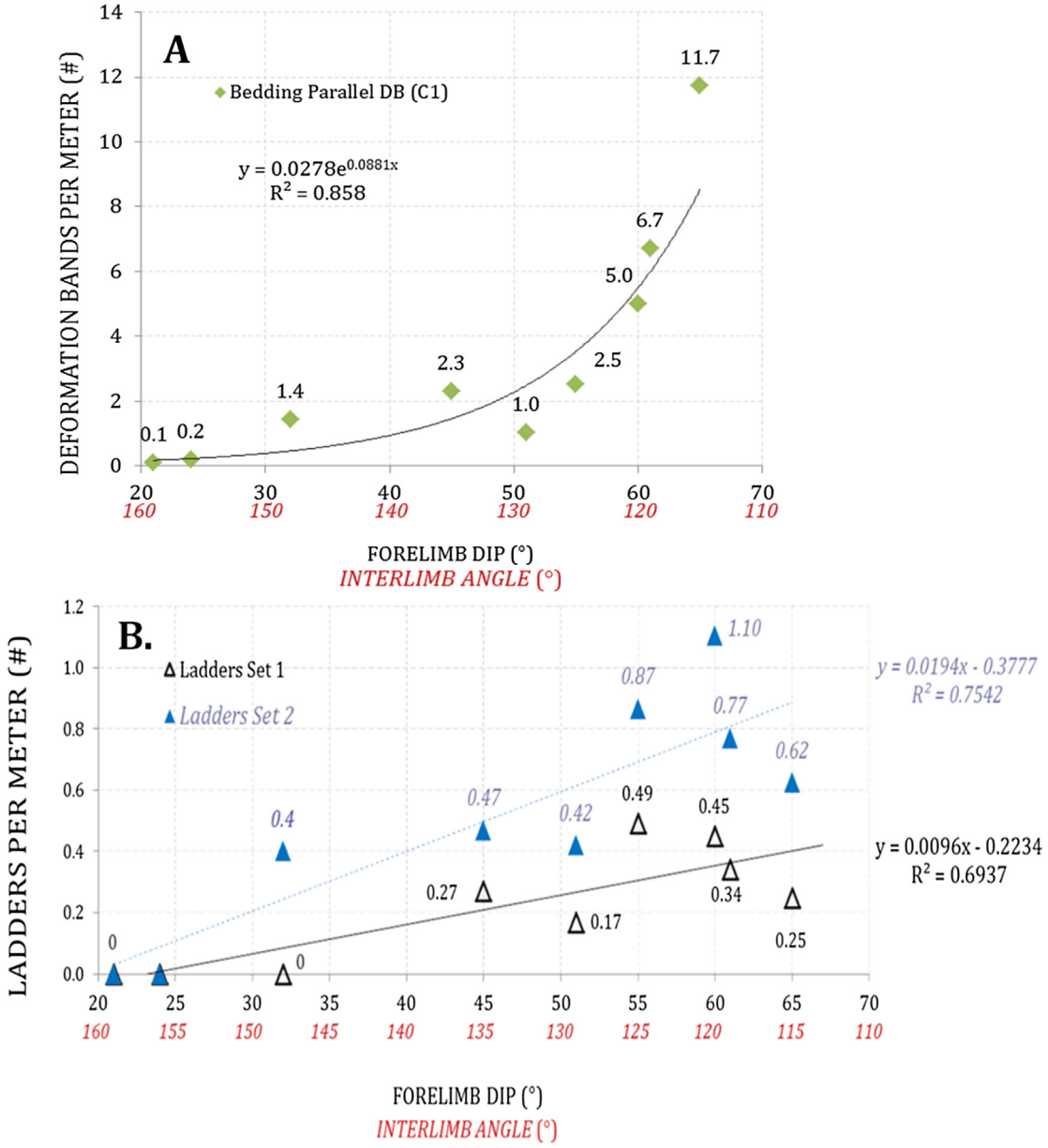

Fig. 8. Deformation bands per unit length with respect to forelimb dips and interlimb angles for (A) bedding-parallel deformation bands C1, and (B) conjugate sets of ladder structures C2; Set 1 corresponds to ladders dipping steeply towards the west, whereas Set 2 is from flat to gently eastward-dipping ladders (see C2 sets in Fig. 7). Increase is exponential for bedding-parallel bands, while ladders exhibit linear growth. Categories 3 and 4 are not shown.

overview of the sandstone permeability from base to top. The probe permeameter measurements indicate that, in the absence of local cementation, host rock permeability for the Navajo sandstone in the SRM ranges from 600 to 900 mD on average, reaching maximums of around 3.5 darcy (Fig. 9A). Deformation bands in turn yield values usually below 100 mD (Fig. 9B).

Probe permeameter measurements from deformation band-host rock pairs show a reduction of permeability by up to two orders of magnitude (Fig. 9D), one order being more common, which is also shown by the frequency distribution histograms extracted from the entire dataset (Fig. 9A, B). There are limitations and uncertainties involved in measuring deformation band permeability with a probe permeameter, notably the lack of confinement of the sample and eventual leakage in the nozzle, and a former study revealed that standard laboratory plug measurements tend to be ~1.8 times the TinyPerm II measurements (Fossen et al., 2011). Nevertheless, the measurements reveal significant reductions in permeability associated with deformation bands.

Thin section analyses from samples in the steep domains show porosity averages of 20.3% for intact host rock and 6% for host rock containing deformation bands in the steepest dip domain (Fig. 9C). The main mechanism for porosity reduction within the bands is mechanical compaction associated with cataclasis, with cementation and pressure solution playing an additional but smaller role.

6. Strain analysis at micro and macroscale

Strain at the grain scale is produced by anisotropic volume change (compaction and pressure solution) caused by grain reorganization and dissolution at grain contact points; due to the shallow burial (2–3 km) of the Navajo Sandstone in this area the pressure solution is likely influenced by tectonic loading rather than being formed by vertical mechanical compaction alone. Evidence of pressure solution is seen both in the host rock and in the bands, and in order to investigate and quantify any strain related to pressure solution, the center to center or Fry method (Waldron and Wallace, 2007) was employed. Thin sections from the steep dip domain where chosen, in which grain center points in host rock away from deformation bands were marked and used for the analysis of potential pressure solution undisturbed by cataclasis. The results reveal 2D strain ellipses with ellipticities of $R = 1.4$ to 1.6 (Fig. 10). Analysis of deformation bands in ladder zones reveal that at outcrop scale, strain is accommodated by a combination of semi-brittle and ductile shear (by means of granular rearrangements at the host rock that preserve relative continuity of bedding), while failure is represented by the deformation band arrays.

For fold-scale strain considerations, a trishear model was developed following the assumptions summarized in Hardy and Allmendinger (2011) to explore how modeled fold-related strain compares with the thin section-scale results from the Fry analysis. Trishear is a purely kinematic model that excludes any mechanical heterogeneities that may exist in the rocks, and where displacement is distributed in a triangular zone ahead of a propagating fault tip (see Allmendinger, 1998 for details). In the trishear model, stratigraphic thicknesses are maintained at the edges of the model, whereas in the triangular fault-propagation fold zone, beds are progressively rotated, thinned and strained.

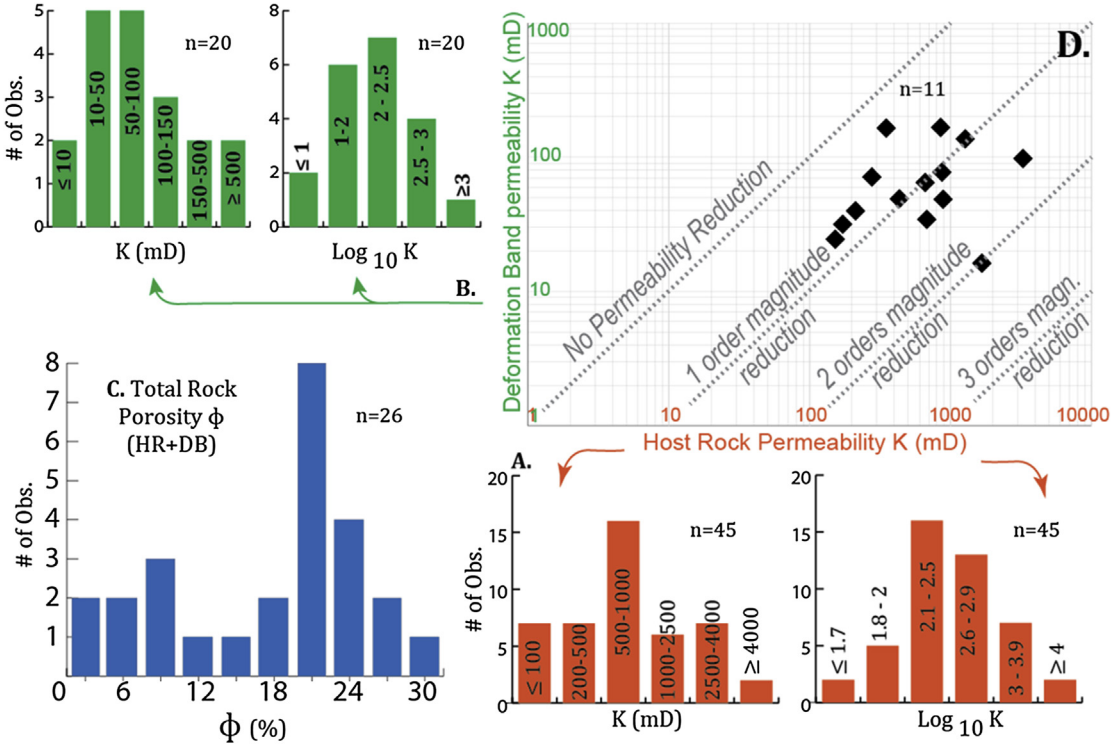

Fig. 9. Petrophysical measurements for the Navajo Sandstone in the study area. In histograms vertical axis are number of observations, horizontal axis are measurements sorted into bin widths. Bottom right (A) and Top left (B): skewed normal and log normal histograms for permeability (all data, Tiny-Perm measurements) showing statistical distributions of permeability for intact host rock (A, orange bars), and individual deformation bands (B, green bars). Permeability of intact host rock has recurrent values of 500 mD to 1 darcy, and reaches maximums of 4 darcy, whereas deformation band common values ranges between 30 and 50 mD. C. Bottom left: porosity distributions of the Navajo Sandstone in the SRR, from 26 thin section analyses of six samples collected in steep dip domains. Porosity shows bimodal distribution, with highest peak of around 20% for intact host rock and lower peak for host rock containing deformation band arrays, reducing porosity to values below 10% (reduction of one order of magnitude). D. Top right: permeability measurements of 11 pairs of deformation band/adjacent host rock, displaying host rock permeability reductions of up to 2 orders of magnitude. (For interpretation of the references to color in this figure legend, the reader is referred to the web version of this article.)

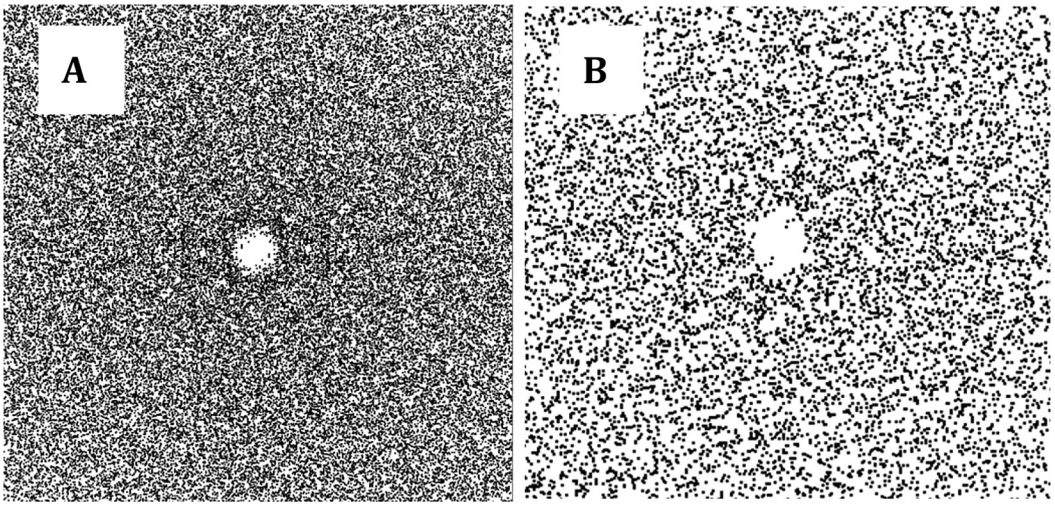

Fig. 10. Fry plots showing elliptical vacancies of grain center distributions in intact host rock using thin sections in (A) optical microscopy, and (B) electron microscopy. Resulting sectional strain ellipses ($R = 1.4$ and 1.6); both shear zones are right lateral and east verging.

In our model, the propagating fault affects Cambrian, Mississippian and Permian intervals at depth, but we stop the propagation before the tip reaches the Navajo Sandstone (Fig. 11). Using an apical angle of 40°, a propagation-to-slip ratio of 1.2, and a 60° fault dip, we ran the model until the Navajo geometry in the model attained the maximum dip identified in the field (Fig. 11, bottom). The usage of a sine velocity field for the trishear zone prevents the occurrence of kink-like bends. The fit between the model and the mapped geometry of the Navajo is good, although the present structural relief of the monocline was slightly underrepresented in the model (1.1 km in the model vs. 1.2 km in the field).

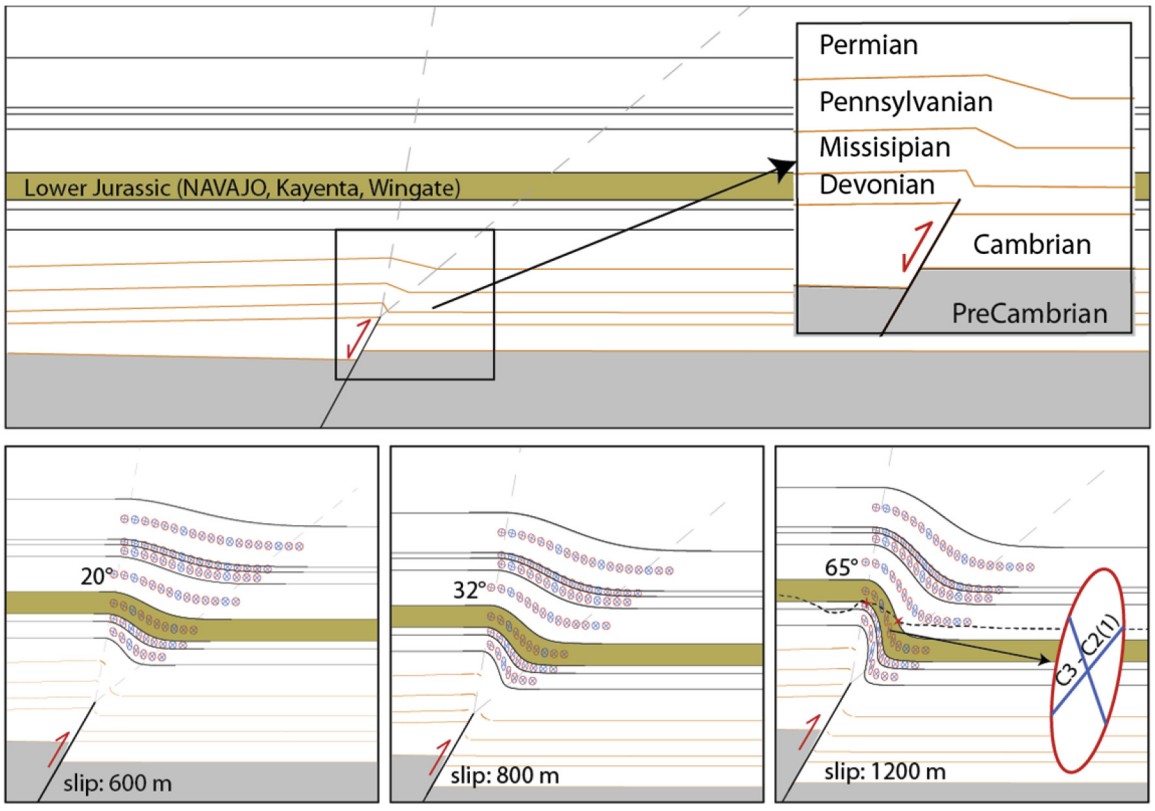

Fig. 11. Trishear model of SRM. Top: initial stage of the model before Laramide episode (detail of middle Paleozoic inversion); bottom: model at 600, 800 and 1200 m of slip resulting in 20°, 32° and 65° of dip at the Navajo interval respectively. Strain is highest near the tip zone from the triangular zone, decreasing towards the backlimb and ahead of the forelimb; the lines of no finite elongation dipping towards the fold core correspond approximately to the west-dipping set 1 of ladder structures seen in the field (Category 2), or the slip surfaces at the base of the unit (Category 4). The enlarged ellipse from the trishear model was chosen to match the forelimb segment that outcrops in the steepest canyons of the SRM. *Models developed using Fault Fold Forward software © v.6.*

In terms of two-dimensional strain, when comparing strain ellipses between scales, trishear strain ellipses for final stages located at the forelimb segment (Fig. 11 bottom right) show ellipticities of $R = 2.6$. This number is significantly higher than what was obtained from the microscale Fry method ($R = 1.4–1.6$), because it represents the total strain that in reality is partitioned between deformation band structures (shear and some compaction) and pressure solution of the sandstone between the deformation band structures.

Trishear models are entirely kinematic, they do not account for layer parallel shear and disregards mechanical contrasts. However, it is interesting that the orientation of the strain ellipse from the Fry method sampled at the forelimb of the SRM is similar to that of the forelimb segment of the trishear model, suggesting that the pressure solution captured by the host rock is related to the formation of the SRM and not by vertical mechanical compaction or other tectonic episodes other than Laramide.

In the progressive folding model presented in this work, domains of different limb dips are associated with different amounts of slip on the controlling fault, and therefore different evolutionary stages, and different amounts of strain. These stages correspond to **a)** the onset of bedding-parallel deformation bands, which is identified in localities with 25° of forelimb dip (600 m of fault slip), **b)** the initiation of ladder zones, identified in the field at forelimb dip values of 32° or higher, corresponding to a fault slip of 800 m in the model, and **c)** the region of highest dips, where the forelimb dips 65°, corresponding to 1260 m of fault slip in the trishear model. At the latter stages, the model fault tip has propagated into the Mississippian strata, consistent with observations from the East Kaibab monocline southwest of the San Rafael Swell (Timmons and Karlstrom, 2012).

7. Discussion

The formation of the San Rafael monocline led to a variety of deformation structures at different stages and scales, each of which are influenced or controlled by lithology, rheology, strain rate and state of stress. This study presents an analysis of populations of cataclastic deformation bands present in the forelimb of the San Rafael monocline, exploring the effect of fault-propagation folding on porous sandstone. Our observations reveal a progressive increase in number and thickness of deformation bands, as well as a change in character and spatial arrangements, as the fold tightens and the forelimb steepens. This allows us to interpret a sequence of deformation band formation through time and for different stages of fold growth and strain. Most previous work on deformation band distribution have focused on their relationship with faults and fault damage zones, particularly their density as a function of the distance to the fault core (e.g., Schueller et al., 2013). The results of the dip domain approach employed in the present work can be applied to predict types and abundance of deformation bands in settings of fault propagation zones, with deformation bands formed due to folding strain in porous layers.

7.1. Temporal evolution of deformation bands

Each dip domain recognized in the field can be correlated with a specific stage of folding in response to an underlying fault displacement. In other words, gentle dip domains represent initial stages of fold growth, while steeper dip domains exhibit a more advanced record of deformation structures. Hence, we can gain insight into the progressive evolution of outcrop-scale structures by comparing the different dip domains.

The strain development can be interpreted from the data according to the following stages (Fig. 12): **i)** In the first stage, lithology contrasts inside the sandstone, such as crossbeds and duneset boundaries, create nucleation sites for deformation bands that gradually grow and join to form thicker strands of Category 1 (Fig. 12-1). **ii)** In the second stage, as strain increases, these sedimentological contrasts begin to play a subordinate role, and deformation bands develop into conjugate sets of ladder zones (Category 2) that transect bedding and dunesets as well as the former bedding-parallel deformation bands (Fig. 12-2). **iii)** Continuing strain widens and rotates all preexisting deformation bands, further developing the ladder zones in terms of number and complexity (Fig. 12-3). Finally, **iv)** strain localized at the boundary between the Navajo Sandstone and its mechanically different overlying and underlying formations results in thick clusters of deformation bands near (and sub-parallel to) the top of the formation (Category 4), which we relate to flexural slip between the Navajo Sandstone and the less competent Chinle Formation. Simultaneously, the interaction with the underlying Kayenta Formation might result in higher cementation of the Navajo Sandstone and the formation of late stage slip surfaces (Category 3) as seen in Fig. 12-3.

Our observations show that bedding-parallel deformation bands always form first, and continue to accumulate exponentially as the steep limb rotates. Ladder zones start to form as more strain is accumulating, and continue to grow in a semi-linear fashion, until a point at which they stop increasing in number, but continue to grow thicker. At this point a characteristic spacing of ladder zones is achieved, which for the Navajo Sandstone is about 3–5 m (distance between each zone). This value is probably controlled by both layer thickness and/or sandstone properties, although the details are not known.

Lastly, mechanical contrasts (Navajo-Kayenta at the base, Navajo-Carmel at top), begin to play a more important role as strain of the Navajo increases. The occurrence of categories 3 and 4, restricted to steep dip domains, could be a response to a shift between strain localization within the Navajo becoming influenced by external boundary conditions, i.e. a stronger external effect of friction and flexural slip where the boundaries between formations play a more significant role in accommodating strain.

The orientation patterns of different categories of deformation bands have undergone clockwise rotations up to 40°, this maximum rotation experienced by the early-stage bedding parallel bands (C1), followed by ladder zone rotations of ~30° (see Fig. 4C). The least amount of rotation, from zero to 10°–15°, is experienced by categories 3 and 4 respectively, as they formed last (Fig. 4B). C3 and C4 are present in steep dip domains only, and Category 4 is not entirely parallel to bedding, thus more spread is shown in their orientations, in addition, some of these rotations are responsible for the apparent normal displacement of few ladder zones.

The strain analysis indicate that some strain is accommodated by the host rock, as shown by means of the center to center method, while a larger component of strain is accommodated by deformation band formation. One of the lines of no finite elongation from the trishear model (Fig. 11), which are proxies for potential shear plane orientation (Hardy and Allmendinger, 2011) matches the orientations of linking bands in ladder structures (east dipping line of no finite elongation; l.n.f.e.), whereas the west-dipping l.n.f.e. roughly corresponds to the west-dipping set of ladder zones, as well as the slip surfaces (Category 3 structures) at the base of the Navajo Sandstone.

7.2. Deformation bands and stress orientation

One of the key questions when it comes to monoclines and paleostress and strain is how much the structures rotated after

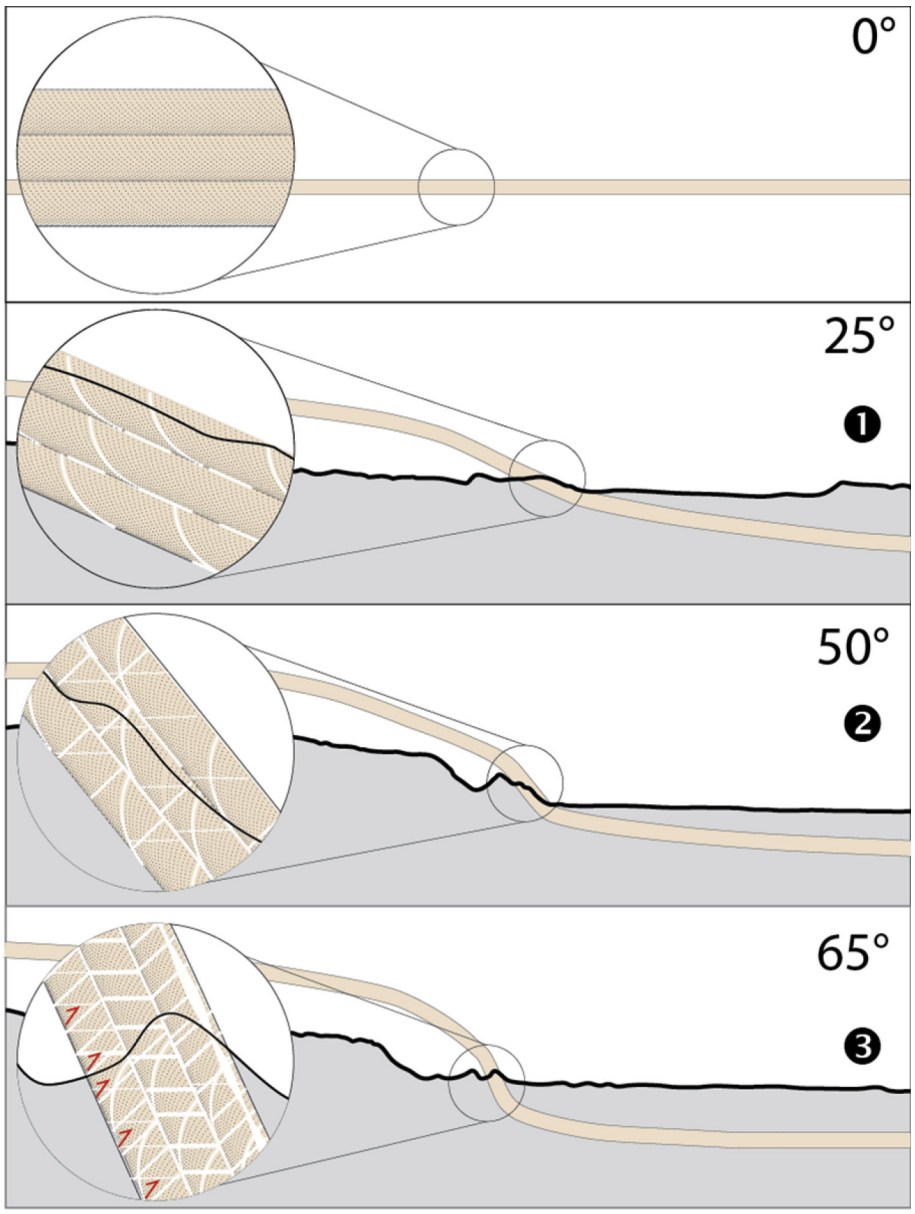

Fig. 12. Proposed evolution of deformation bands in the San Rafael monocline (Navajo interval constructed above and below present day topography in gray). Bedding-parallel and crossbed-parallel deformation bands begin forming at gentle dip domains (❶), ladder structures, cutting across bedding occur as folding progresses (❷). Deformation bands continue to develop, increasing in thickness and number. At final stages, clusters aggregate at the top of the unit, whereas slip surfaces form at the base of the formation (❸).

their formation. The evolutionary model delineated above implies that the bedding-parallel bands (Category 1) rotated up to 40°. The first formed ladder structures, forming at forelimb dips of 32°, may have rotated up to 33° in the steepest parts of the SRM, although younger ladder structures would have rotated less. Comparing ladder zones in the medium-dip domain with those in the high-dip domain (Fig. 4D) shows a significant difference in orientations that can be corrected for by a ca. 30° counterclockwise rotation, consistent with the sense of rotation predicted by the progressive folding model (Fig. 11).

The slip surfaces, forming along existing deformation band zones, were the last structures to form, and probably did not rotate much. They are therefore most directly related to the stress field during (late stages of) folding. The slickensides (Category 3) suggest top-to the E or ESE sense of slip (Fig. 4B), perpendicular to the trend of the monocline. This is consistent with the general WNW–ESE principal compressional stress or shortening direction reported by previous workers (Davis, 1999a; Bump and Davis, 2003; Fischer and Christensen, 2004). Although individual deformation bands do not allow for a definite identification of the local maximum shortening direction or the maximum principal stress (σ_1), an estimate can be made from the bisecting planes between conjugate sets of ladder zones (Fig. 4C). After 33° of rotation, to reach a bedding dip of 32° (i.e. initiation of ladder zones), values returned $\sigma_1 = 313°$, a NW–SE horizontal contraction comparable to the values of reported by Fischer and Christensen (2004) in their fracture analysis of the same area ($\sigma_1 = 284°$).

Antonellini and Aydin (1995) in their study of an extensionally-derived fault propagation structure in Arches National Park found maximum density of deformation bands in the zone of maximum curvature of the folded strata, comparable to the San Rafael monocline steep dip domains, that also contain highest density of deformation bands, albeit our structure is in a less developed stage of fault propagation.

7.3. Applications

The findings above pertain to subsurface reservoirs where folds, notably fault-propagation folds, can be mapped from seismic data and where deformation band structures are expected to be present, but at the subseismic scale. Folding of layers always implies internal deformation of layers, but exactly how this strain is expressed in terms of structures and structural variation depends on several factors. In general terms, low burial depths (poor lithification) and overpressure favor non-destructive strain by means of non-cataclastic granular flow. In this case grains simply rotate or shift slightly to accommodate the strain related to folding, and/or non-cataclastic deformation bands (disaggregation bands) evolve. The effect of this deformation on fluid flow is generally low (Fisher and Knipe, 2001).

However, cataclastic deformation bands of the type found in the San Rafael monocline form at deeper depths, generally below 1 km, but in some cases at shallower burial depths (e.g., Ballas et al., 2012b). In reservoirs with cataclastic bands the relationship between strain or forelimb dip with deformation band geometry can be used to predict subsurface deformation in relation to fold geometry. It is interesting that not only the hinge zones (areas of maximum curvature) but also the steep limb is strained in the monocline, as predicted by the trishear model. The alternative model, where strain is localized to the hinge zones and the short limb rotates with less internal strain, does not fit our observations from the San Rafael monocline, implying that strain or deformation band density correlates with dip rather than with curvature. Attempting a curvature analysis in which sampling the continuous horizon at discrete points is needed (Lisle, 1994), is not a good approach for a predictive model of the present example, as the upper and lower hinges of the SRM are respectively eroded and buried, and even though the steep limb is widely exposed, the Navajo sandstone does not show any significant curvature in these exposed sections.

Dip slip vs. oblique slip can differently affect the localization of deformation; for the East Kaibab monocline, which is a product of reverse right lateral faulting (Tindall and Davis, 1999) deformation is localized in the hinges, in a tangential longitudinal strain fashion, while the SRM on the other hand suggests flexural flow with strain in the rotated steep limb.

8. Conclusions

Through a detailed study of several well-exposed outcrops of the San Rafael monocline, the present work has focused on the relationship between the geometry and evolution of contractional fault propagation folds, and the distribution of discrete strain in the form of deformation bands. We uncovered a close relationship between fold tightness (reflected by the dip of the forelimb) and the intensity and types of deformation band structures along strike, as a response to the various evolutionary stages of the San Rafael monocline's fault propagation during the ESE–WNW Laramide shortening. We conclude that the growth of the studied contractional fault propagation folds was accompanied by the nucleation and growth of progressively more complex deformation band arrays: Throughout the growth history of the fold, bed-parallel deformation bands were the first strain localization structures to form, then as the forelimb dip exceeded 25°, deformation band zones showing ladder structures started to form, which evolved into a conjugate network of ladder zones as the forelimb dip exceeded 32°. As forelimb dips became increasingly steeper (up to 65°), the deformation band complexity and density peaked with the formation of decimeter-thick deformation band ladder zones.

The findings of this study offer new insights to the fundamentals of discrete strain localization in contractional fault propagation folds. Furthermore, our results have implications of potential economic significance. The observed correlation between fold tightness (dip of steep limb layers) and deformation band density offers insight that may be applied to predicting deformation band occurrence in structurally similar subsurface settings, i.e. where contractional fault propagation faults exist at depth but where the limitation of seismic resolution prevents the detection of smaller-scale structures. Given that deformation bands generally have a negative effect on fluid flow (e.g. Fossen et al., 2007), this is may be of relevance in the management of structurally similar petroleum, CO_2 and groundwater reservoirs (cf. Rotevatn and Fossen, 2011).

Acknowledgments

This manuscript was greatly improved by reviews from George H. Davis, Juliet Crider and initial remarks by David Peacock. This work is part of the COPS project (contraction of porous sandstones) at the Centre for integrated petroleum research (Uni CIPR), supported by the University of Bergen and Statoil. Tracy Joseph Johnson is thanked for his companionship in the field. Colleagues at Uni CIPR provided useful feedback and discussions. Information publicly available online was downloaded from the Utah Geological Survey and The Utah Automated Geographic Reference Center.

Appendix A. Supplementary data

Supplementary data related to this article can be found at http://dx.doi.org/10.1016/j.jsg.2014.09.008.

References

Ahlgren, S.G., 2001. The nucleation and evolution of Riedel shear zones as deformation bands in porous sandstone. J. Struct. Geol. 23 (8), 1203–1214.
Allen, P.A., Verlander, J.E., Burgess, P.M., Audet, D.M., 2000. Jurassic giant erg deposits, flexure of the United States continental interior, and timing of the onset of Cordilleran shortening. Geology 28 (2), 159–162.
Allmendinger, R.W., 1992. Fold and thrust tectonics of the western United States exclusive of the accreted terranes. In: The Cordilleran Orogen: Conterminous US. Geology of North America, vol. 3. Geological Society of America, Boulder, Colorado, pp. 583–607.
Allmendinger, R.W., 1998. Inverse and forward numerical modeling of trishear fault-propagation folds. Tectonics 17, 640–656.
Antonellini, M., Aydin, A., 1994. Effect of faulting on fluid flow in porous sandstones: petrophysical properties. Am. Assoc. Pet. Geol. Bull. 78, 355–377.
Antonellini, M., Aydin, A., 1995. Effect of faulting on fluid flow in porous sandstones: geometry and spatial distribution. Am. Assoc. Pet. Geol. Bull. 79, 642–671.
Antonellini, M.A., Aydin, A., Pollard, D.D., 1994. Microstructure of deformation bands in porous sandstones at Arches National Park, Utah. J. Struct. Geol. 16, 941–959.
Aydin, A., 1977. Small faults formed as deformation bands in sandstone. In: Evernden, J.F. (Ed.), Proceedings of Conference II; Experimental Studies of Rock Friction with Application to Earthquake Prediction. U. S. Geol. Surv., Off. Earthquake Stud., Menlo Park, Calif., pp. 617–653.
Aydin, A., 1978. Small faults formed as deformation bands in sandstone. Pure Appl. Geophys. 116, 913–930.
Aydin, A., Ahmadov, R., 2009. Bed-parallel compaction bands in aeolian sandstone: their identification, characterization and implications. Tectonophysics 479, 277–284.
Aydin, A., Borja, R.I., Eichhubl, P., 2006. Geological and mathematical framework for failure modes in granular rock. J. Struct. Geol. 28 (1), 83–98.
Aydin, A., Johnson, A.M., 1977. Development of Faults as Zones of Deformation Bands and as Slip Surfaces in Sandstone. U. S. Geol. Surv., Off. Earthquake Stud., Menlo Park, Calif.
Aydin, A., Johnson, A.M., 1978. Development of faults as zones of deformation bands and as slip surfaces in sandstones. Pure Appl. Geophys. 116 (4–5), 931–942.
Aydin, A., Reches, Z., 1982. The number and orientation of fault sets in the field and in experiments. Geology 10, 107–112.
Ballas, G., Soliva, R., Sizun, J.-P., Benedicto, A., 2012a. Impact of deformation bands on subsurface fluid flow (Provence, France). In: EGU General Assembly 2012 14, Vienna, Austria.
Ballas, G., Soliva, R., Sizun, J.-P., Benedicto, A., Cavailhes, T., Raynaud, S., 2012b. The importance of the degree of cataclasis in shear bands for fluid flow in porous sandstone, Provence, France. AAPG Bull. 96 (11), 2167–2186.

Beitler, B., Chan, M.A., Parry, W.T., 2003. Bleaching of Jurassic Navajo Sandstone on Colorado Plateau Laramide highs: evidence of exhumed hydrocarbon supergiants? Geology 31 (12), 1041–1044.
Beitler, B., Parry, W.T., Chan, M.A., 2005. Fingerprints of fluid flow: chemical diagenetic history of the Jurassic Navajo Sandstone, southern Utah, U.S.A. J. Sediment. Res. 75 (4), 547–561.
Bésuelle, P., 2001. Evolution of strain localisation with stress in a sandstone: brittle and semi-brittle regimes. Phys. Chem. Earth 26, 101–106.
Bjerrum, C.J., Dorsey, R.J., 1995. Tectonic controls on deposition of Middle Jurassic strata in a retroarc foreland basin, Utah-Idaho Trough, Western Interior, United States. Tectonics 14 (4), 962–978.
Blakey, R.C., Middleton, L.T., 2012. Geologic history and paleogeography of Paleozoic and early Mesozoic sedimentary rocks, eastern Grand Canyon, Arizona. Geol. Soc. Am. Spec. Pap. 489, 81–92.
BLM, USGS, 2005. San Rafael Swell – Trail Map 712. National Geographic – Trails Ilustrated Maps.
Brandenburg, J.P., Alpak, F.O., Solum, J.G., Naruk, S.J., 2012. A kinematic trishear model to predict deformation bands in a fault-propagation fold, East Kaibab monocline, Utah. AAPG Bull. 96 (1), 109–132.
Brandenburg, J.P., Solum, J.G., Kostenko, O.V., Naruk, S., Schultz, R.A., Anonymous, 2009. Deformation band networks in Mesozoic eolian sandstones of the western United States and offshore hydrocarbon reservoirs. In: Abstracts: Annual Meeting – American Association of Petroleum Geologists 2009.
Bump, A.P., Davis, G.H., 2003. Late Cretaceous–early Tertiary Laramide deformation of the northern Colorado Plateau, Utah and Colorado. J. Struct. Geol. 25 (3), 421–440.
Cashman, S., Cashman, K., 2000. Cataclasis and deformation-band formation in unconsolidated marine terrace sand, Humboldt County, California. Geology 28 (2), 111–114.
Condon, S.M., Huffman, A., 1997. Geology of the Pennsylvanian and Permian Cutler Group and Permian Kaibab Limestone in the Paradox Basin, Southeastern Utah and Southwestern Colorado. US Government Printing Office.
Cross, T.A., 2009. Tectonic controls of foreland basin subsidence and Laramide style deformation, western United States. In: Foreland Basins. Blackwell Publishing Ltd., pp. 13–39.
Davatzes, N.C., Aydin, A., Eichhubl, P., 2003. Overprinting faulting mechanisms during the development of multiple fault sets in sandstone, Chimney Rock fault array, Utah, USA. Tectonophysics 363, 1–18.
Davis, G.H., 1998. Fault-fin landscape. Geol. Mag. 135 (2), 283–286.
Davis, G.H., 1999a. Colorado Plateau intraplate deformation as expressed by systems of deformation bands. Abstr. Progr. Geol. Soc. Am. 31 (7), 238.
Davis, G.H., 1999b. Structural geology of the Colorado Plateau Region of southern Utah, with special emphasis on deformation bands. Geol. Soc. Am. Spec. Pap. 342, 1–157.
Davis, G.H., Bump, A.P., 2009. Structural geologic evolution of the Colorado Plateau. In: Kay, S.M., Ramos, V.A., Dickinson, W.R. (Eds.), Backbone of the Americas: Shallow Subduction, Plateau Uplift, and Ridge and Terrane Collision, Geological Society of America Memoir, vol. 204, pp. 99–124.
Davis, G.H., Bump, A.P., Garcia, P.E., Ahlgren, S.G., 2000. Conjugate Riedel deformation band shear zones. J. Struct. Geol. 22, 169–190.
DeCelles, P.G., Coogan, J.C., 2006. Regional structure and kinematic history of the Sevier fold-and-thrust belt, central Utah. Geol. Soc. Am. Bull. 118, 841–864.
Dickinson, W., Snyder, W., 1978. Plate tectonics of the Laramide orogeny. Geol. Soc. Am. Mem. 151, 355–366.
Du Bernard, X., Eichhubl, P., Aydin, A., 2002. Dilation bands: a new form of localized failure in granular media. Geophys. Res. Lett. 29, 2176–2179.
Dumitru, T.A., Duddy, I.R., Green, P.F., 1994. Mesozoic–Cenozoic burial, uplift, and erosion history of the west-central Colorado Plateau. Geology 22, 499–502.
Filomena, C., Hornung, J., Stollhofen, H., 2014. Assessing accuracy of gas-driven permeability measurements: a comparative study of diverse Hassler-cell and probe permeameter devices. Solid Earth 5 (1).
Fischer, M.P., Christensen, R.D., 2004. Insights into the growth of basement uplifts deduced from a study of fracture systems in the San Rafael monocline, east central Utah. Tectonics 23 (1), TC1018.
Fisher, Q.J., Knipe, R.J., 2001. The permeability of faults within siliciclastic petroleum reservoirs of the North Sea and Norwegian Continental Shelf. Mar. Pet. Geol. 18, 1063–1081.
Fossen, H., Bale, A., 2007. Deformation bands and their influence on fluid flow. Am. Assoc. Pet. Geol. Bull. 91, 1685–1700.
Fossen, H., Hesthammer, J., 1997. Geometric analysis and scaling relations of deformation bands in porous sandstone. J. Struct. Geol. 19, 1479–1493.
Fossen, H., Rotevatn, A., 2012. Characterization of deformation bands associated with normal and reverse stress states in the Navajo Sandstone, Utah: discussion. AAPG Bull. 96 (5), 869–876.
Fossen, H., Schultz, R.A., Rundhovde, E., Rotevatn, A., Buckley, S.J., 2010. Fault linkage and graben stepovers in the Canyonlands (Utah) and the North Sea Viking Graben, with implications for hydrocarbon migration and accumulation. Am. Assoc. Pet. Geol. Bull. 94, 597–613.
Fossen, H., Schultz, R.A., Shipton, Z.K., Mair, K., 2007. Deformation bands in sandstone: a review. J. Geol. Soc. 164, 755–769.
Fossen, H., Schultz, R.A., Torabi, A., 2011. Conditions and implications for compaction band formation in the Navajo Sandstone, Utah. J. Struct. Geol. 33, 14.
Goldstrand, P.M., 1994. Tectonic development of Upper Cretaceous to Eocene strata of southwestern Utah. Geol. Soc. Am. Bull. 106, 145–154.
Hardy, S., Allmendinger, R.W., 2011. Trishear: a Review of Kinematics, Mechanics, and Applications.
Herman, G., Sharps, S.L., 1956. Pennsylvanian and Permian Stratigraphy of the Paradox Salt Embayment.
Hesthammer, J., Johansen, T.E.S., Watts, L., 2000. Spatial relationships within fault damage zones in sandstone. Mar. Pet. Geol. 17, 873–893.
Huntoon, J., Dubiel, R., Stanesco, J., 1994. Tectonic influence on development of the Permian–Triassic unconformity and basal Triassic strata, Paradox basin, southeastern Utah. In: Mesozoic Systems of the Rocky Mountain Region. SEPM, Rocky Mountain Section, USA, pp. 109–131.
Huntoon, P.W., 1993. Influence of inherited Precambrian basement structure on the localization and form of Laramide monoclines, Grand Canyon, Arizona. Spec. Pap.-Geol. Soc. Am. 243.
Jamison, W.R., 1989. Fault-fracture strain in Wingate Sandstone. J. Struct. Geol. 11, 959–974.
Johansen, S.E., Fossen, H., 2008. Internal geometry of fault damage zones in siliciclastic rocks. In: Wibberley, C.A.J., Kurz, W., Imber, J., Holdsworth, R.E., Collettini, C. (Eds.), The Internal Structure of Fault Zones: Implications for Mechanical and Fluid-Flow Properties, Geological Society Special Publication, vol. 299, pp. 35–56.
Johnson, K.M., Johnson, A.M., 2000. Localization of layer-parallel faults in San Rafael swell, Utah and other monoclinal folds. J. Struct. Geol. 22, 1455–1468.
Jones, C.H., Farmer, G.L., Sageman, B., Zhong, S., 2011. Hydrodynamic mechanism for the Laramide orogeny. Geosphere 7 (1), 183–201.
Karlstrom, K.E., Timmons, J.M., 2012. Faulting and uplift in the Grand Canyon Region. In: Grand Canyon Geology: Two Billion Years of Earth's History, vol. 489, p. 93.
Lisle, R., 1994. Detection of zones of abnormal strains in structures using gaussian curvature analysis. AAPG Bull. 78, 1811–1819.
Marshak, S., Nelson, W.J., McBride, J.H., 2003. Phanerozoic strike-slip faulting in the continental interior platform of the United States: examples from the Laramide Orogen, Midcontinent, and Ancestral Rocky Mountains. In: Storti, F., Holdsworth, R.E., Salvini, F. (Eds.), Intraplate Strike-Slip Deformation Belts, Geological Society, London, Special Publications, vol. 210, pp. 159–184.
Miall, A.D., Blakey, R.C., 2008. The Phanerozoic tectonic and sedimentary evolution of North America (Chapter 1). In: Andrew, D.M. (Ed.), Sedimentary Basins of the World, vol. 5. Elsevier, pp. 1–29.
Neuhauser, K.R., 1988. Sevier-age ramp-style thrust faults at Cedar mountain, northwestern San Rafael swell (Colorado Plateau), Emery County, Utah. Geology 16, 299–302.
Nuccio, V.F., Condon, S.M., 2000. USGS Bulletin 2000-O: Burial and Thermal History of the Paradox Basin, Utah and Colorado, and Petroleum Potential of the Middle Pennsylvanian Paradox Basin. U.S., 41.
Okubo, C.H., Schultz, R.A., Fossen, H., Hesthammer, J., 2006. Near-tip stress rotation and the development of deformation band stepover geometries in mode II. Geol. Soc. Am. Bull. 118 (3–4), 343–348.
Parry, W.T., Chan, M.A., Nash, B.P., 2009. Diagenetic characteristics of the Jurassic Navajo Sandstone in the Covenant oil field, central Utah thrust belt. Am. Assoc. Pet. Geol. Bull. 93, 1039–1061.
Rigby, J.K., 1987. Stratigraphy and structure of the San Rafael Reef, Utah; a major monocline of the Colorado Plateau. Geol. Soc. Am. Centen. Field Guide – Rocky Mt. Sect. 269–273.
Rotevatn, A., Fossen, H., 2011. Simulating the effect of subseismic fault tails and process zones in a siliciclastic reservoir analogue: implications for aquifer support and trap definition. Mar. Pet. Geol. 28 (9), 1648–1662.
Rotevatn, A., Sandve, T., Keilegavlen, E., Kolyukhin, D., Fossen, H., 2013. Deformation bands and their impact on fluid flow in sandstone reservoirs: the role of natural thickness variations. Geofluids 13 (3), 359–371.
Rotevatn, A., Tveranger, J., Howell, J.A., Fossen, H., 2009. Dynamic investigation of the effect of a relay ramp on simulated fluid flow: geocellular modelling of the Delicate Arch Ramp, Utah. Pet. Geosci. 15, 45–58.
Saillet, E., Wibberley, C.A., 2013. Permeability and flow impact of faults and deformation bands in high-porosity sand reservoirs: Southeast Basin, France, analog. AAPG Bull. 97 (3), 437–464.
Saillet, E., Wibberley, C.A.J., 2010. Evolution of cataclastic faulting in high-porosity sandstone, Bassin du Sud-Est, Provence, France. J. Struct. Geol. 32, 1590–1608.
Schueller, S., Braathen, A., Fossen, H., Tveranger, J., 2013. Spatial distribution of deformation bands in damage zones of extensional faults in porous sandstones: statistical analysis of field data. J. Struct. Geol. 52, 148–162.
Schultz, R.A., Balasko, C.M., 2003. Growth of deformation bands into echelon and ladder geometries. J. Geophys. Res. 30.
Shipton, Z.K., Cowie, P., 2001. Damage zone and slip-surface evolution over μm to km scales in high-porosity Navajo sandstone, Utah. J. Struct. Geol. 23, 1825–1844.
Shipton, Z.K., Evans, J.P., Robeson, K., Forster, C.B., Snelgrove, S., 2002. Structural heterogeneity and permeability in faulted aeolian sandstone: implications for subsurface modelling of faults. Am. Assoc. Pet. Geol. Bull. 86, 863–883.
Soliva, R., Schultz, R.A., Ballas, G., Taboada, A., Wibberley, C., Saillet, E., Benedicto, A., 2013. A model of strain localization in porous sandstone as a function of tectonic setting, burial and material properties; new insight from Provence (southern France). J. Struct. Geol. 49, 50–63.
Solum, J.G., Brandenburg, J.P., Naruk, S.J., Kostenko, O.V., Wilkins, S.J., Schultz, R.A., 2010. Characterization of deformation bands associated with normal and reverse stress states in the Navajo Sandstone, Utah. AAPG Bull. 94 (9), 1453–1475.

Stearns, D., Jamison, W., 1977. Deformation of Sandstones over Basement Uplifts, Colorado National Monument.
Sternlof, K., Karimi-Fard, M., Durlofsky, L.J., 2006. Flow and transport effects of compaction bands in sandstone at scales relevant to aquifer and reservoir management. Water Resour. Res. 42, 16.
Timmons, J.M., Karlstrom, K.E., 2012. Grand Canyon Geology: Two Billion Years of Earth's History. Geological Society of America.
Tindall, S.E., 2000. The Cockscomb segment of the East Kaibab monocline: taking the structural Plunge. In: Geology of Utah's Parks and Monuments, vol. 28. Utah Geological Association Publication, p. 15.
Tindall, S.E., Davis, G.H., 1999. Monocline development by oblique-slip fault-propagation folding: the East Kaibab monocline, Colorado Plateau, Utah. J. Struct. Geol. 21, 1303–1320.
Tindall, S.E., Davis, G.H., 2003. Joint spacing and distribution in deformation band shear zones. Geol. Mag. 140, 1–9.
Torabi, A., Fossen, H., 2009. Spatial variation of microstructure and petrophysical properties along deformation bands in reservoir sandstones. Am. Assoc. Pet. Geol. Bull. 93, 919–938.
Tueckmantel, C., Fisher, Q.J., Knipe, R.J., Lickorish, H., Khalil, S.M., 2010. Fault seal prediction of seismic-scale normal faults in porous sandstone: a case study from the eastern Gulf of Suez rift, Egypt. Mar. Pet. Geol. 27 (2), 334–350.
Waldron, J.W.F., Wallace, K.D., 2007. Objective fitting of ellipses in the centre-to-centre (Fry) method of strain analysis. J. Struct. Geol. 29 (9), 1430–1444.
Wibberley, C.A.J., Yielding, G., Di Toro, G., 2008. Recent advances in the understanding of fault zone internal structure: a review. Geol. Soc. Lond. Spec. Publ. 299 (1), 5–33.
Zhao, G., Johnson, A.M., 1992. Sequence of deformations recorded in joints and faults, Arches National Park, Utah. J. Struct. Geol. 14, 225–236.